



Research Article

An experimental study on supersonic jet control using shifted air tabs

Mahendra Perumal GOVINDAN^{1,2,*}, Aravindh Kumar S.M.², Elangovan S.¹, Sundararaj M.¹

¹Department of Aeronautical Engineering, Bharath Institute of Higher Education and Research, Chennai, 600 073, India

²Department of Aerospace Engineering, SRM Institute of Science and Technology, Kattankulathur, Chennai, 603203, India

ARTICLE INFO

Article history

Received: 16 November 2023

Revised: 21 January 2024

Accepted: 24 January 2024

Keywords:

Air Tab; Injection Pressure Ratio; Nozzle Pressure Ratio; Shadowgraph; Supersonic Jet

ABSTRACT

This experimental study investigates the impact of two diametrically positioned sonic air tabs on the mixing characteristics of a Mach 2.1 circular jet. Positioned at an axial distance of $0.25D$ from the convergent-divergent nozzle exit, the air tabs' injection pressure ratio was systematically varied from 3 to 6, while maintaining nozzle pressure ratios of 3, 4, 5, and 6. Through Pitot pressure measurements and flow visualization, the study reveals that the sonic air tabs effectively reduce the core length of the Mach 2.1 jet across all nozzle pressure ratios. The accelerated mixing of the Mach 2.1 jet with the ambient fluid, facilitated by the air tabs, results in shorter core lengths. Importantly, the mixing enhancement by air tabs intensifies with increasing injection pressure ratio for all nozzle pressure ratios, with the maximum reduction in core length consistently occurring at an injection pressure ratio of 6. The observed maximum reductions in core length for nozzle pressure ratios 3, 4, 5, and 6 at an injection pressure ratio of 6 are 41.3%, 60.8%, 43.7%, and 43.5%, respectively. Visualization results confirm the air tabs' effectiveness in attenuating waves within the jet core, with the weakening of waves increasing with higher injection pressure ratios. These findings contribute valuable insights into optimizing supersonic jet performance through fluidic control techniques.

Cite this article as: Govindan MP, Aravindh Kumar SM, Elangovan S, Sundararaj M. An experimental study on supersonic jet control using shifted air tabs. J Ther Eng 2024;10(3):585–598.

INTRODUCTION

Any aerospace vehicle needs an efficient propulsion system to function smoothly across different regimes. Jets exiting from nozzles at high velocities in propulsion systems generate thrust when high-pressure gas expands through a nozzle. Research on jet control focuses on thrust augmentation and thrust vectoring. The mechanical means of thrust vectoring focus on the use of solid grooves, notches, nozzles, tabs, swirls, and chevrons. These structures generate counter-rotating vortices against the normal jet flow,

promoting efficient jet mixing [1, 2]. Several studies have explored the use of tabs of various shapes for controlling high-speed jets [3]. Solid tabs are preferred due to their simple geometry and improved mixing enhancement compared to other techniques [4]. For square tabs, factors like nozzle boundary-layer thickness, turbulence level, and convergence angle have minimal influence on jet development [5]. However, the fixed installation of tabs can impede jet velocity, reduce fuel efficacy, and lead to thrust loss, as they are permanently fixed to the nozzle [6, 7].

*Corresponding author.

*E-mail address: mahendrg@srmist.edu.in

This paper was recommended for publication in revised form by Editor-in-Chief Ahmet Selim Dalkılıç



A more efficient method of thrust vectoring, known as fluidic thrust control or secondary injection, has emerged as a promising jet control strategy following Davis's study in 1982. Jet mixing was achieved by placing two steady injectors separated by 180 degrees at the exit of a Mach 0.8 jet [8, 9]. Over the past 50 years, fluidic injection has been investigated for reducing jet noise sources and modifying jet velocity and temperature profiles [10]. Fluidic injection enhances mixing in the shear layer between the jet plume and its surroundings and offers flexibility in performance by allowing variation of controlling parameters. The increase in mixing caused by the fluidic injectors reduces large-scale noise by increasing turbulent kinetic energy near the nozzle exit [6, 7]. Unlike other control techniques, fluidic injection provides thrust augmentation with mixing enhancement, and the injectors can be activated or deactivated as needed without affecting overall aircraft performance [6, 7, 9]. Additional applications of fluidic injectors include thrust vector control, noise reduction, and drag reduction [9]. Fluidic injection control has greatly helped in reducing vehicle weight, maintenance requirements, and enhancing the stealth characteristics of aircraft, rockets, and missiles [2].

The effect of injection pressure ratio (IPR) on the jet flow characteristics of the supersonic main flow has been an important aspect of research [2]. IPR is defined as the ratio of the stagnation/supply pressure of the secondary jet to the freestream stagnation pressure. In an investigation conducted by Semlitsch and Mihaescu [11], the impact of fluidic injection angles on the mixing properties of a Mach 1.56 jet was examined. The injectors were evenly distributed at the nozzle exit with injector numbers (N) of 6, 12, and 24. The findings indicated that steeper injection angles resulted in enhanced mixing of the jet when compared to shallower injection angles. Similarly, Chauvet et al. [12] through their investigation in underexpanded sonic jet with a nozzle pressure ratio (NPR) of 3.1, proposed that a high IPR/NPR ratio should be utilized to enhance jet mixing and a relatively small value of injector numbers is desirable to avoid premature vortex interaction and excessive diffusion. In a similar study on the effect of the number of injectors (N) on the mixing characteristics of a subsonic jet by Perumal and Zhou [13], it has been concluded that for a given injector diameter to nozzle diameter (d/D) ratio, the rate of jet decay decreases as N increases. In subsonic jets, Yu et al. [14] have demonstrated that the use of air tabs can enhance mixing without causing any thrust loss.

According to Green and McCullough's [15] observation when the pressure of the injected secondary flow relative to the primary flow increases, the efficiency or effectiveness of the propulsion system improves. In other words, as the injection pressure ratio increases, the performance ratio also increases. Also, Rizetta [16] investigated the effect of IPR on the separation length (x_{sep}) and the height of the Mach surface (h_m), wherein both x_{sep} and h_m increased as the IPR increased [2]. Indicating that by increasing the IPR in the jet control system, longer separation lengths and

higher Mach could be achieved. The scaling analysis of a Mach 2.0 jet by Arun Kumar et al. [9] reports that the p_{0c}/p_{0s} decreases as p_e/p_a is reduced and improved control efficiency can be achieved by decreasing the injection diameter by half. Sekar et al. [17] have studied the performance of a converging nozzle with fluid thrust vectoring using secondary jet injection. They reported that the thrust coefficient was dependent on the NPR and mass ratio, while the vector angle was only dependent on the mass ratio and the secondary injection increased the magnitude of the net thrust, while reducing the thrust coefficient.

From the literature, we have understood that there are reasonable experimental studies on supersonic round jets with Mach number ranging from 1.5 to 2. Hence, we wanted to focus on supersonic jet Mach numbers that are less studied. With this aim, we fabricated the nozzle and the Mach number of the jet at the nozzle exit plane was found to be $2.1 \pm .02$. This study introduces a novel exploration into the effects of fluidic injectors on the characteristics of a Mach 2.1 supersonic jet. Employing an innovative fluidic injector design featuring two small control jets, the study aims to emulate the impact of solid tabs while introducing dynamic adjustability into the experimental setup. The main objective of the study was to understand the impact of air tabs on a supersonic jet (Mach 2.1) positioned at an axial distance of $0.25D$ from the nozzle exit while varying the injection pressure ratio (IPR) from 3 to 6 and maintaining a fixed nozzle pressure ratio (NPR) of 3, 4, 5, and 6. The comparison of the core length of the supersonic jet was conducted between configurations with and without air tabs. This analysis involved studying pitot pressure measurements and examining corresponding shadowgraph images of the jets under controlled experimental conditions.

EXPERIMENTAL SETUP

The study was carried out in the open jet facility in the High-Speed Aerodynamics Laboratory, Department of Aerospace Engineering, SRMIST, Chennai. The compressed air from storage tank is made to pass through a ball-valve, pressure regulating valve and 1 m mixing length before reaching the settling chamber. A slot holder is employed to hold the nozzle at the settling chamber exit. The pressure inside the settling chamber (p_{0s}) is regulated using the pressure regulating valve. A separate settling chamber for fluidic injection is used to supply compressed air to the air tabs. The injection settling chamber pressure (p_{0i}) is also controlled using a control valve. During experimentation the pressures in both the chambers are monitored with the help of a pressure scanner. The temperature inside both the chambers is equal to the local atmospheric temperature. Figure 1 shows the schematic of the complete setup used for experiments.

The use of a convergent-divergent nozzle to generate a Mach 2.1 jet with sonic injection at $0.25D$ downstream from the nozzle exit has not been studied previously. In the present

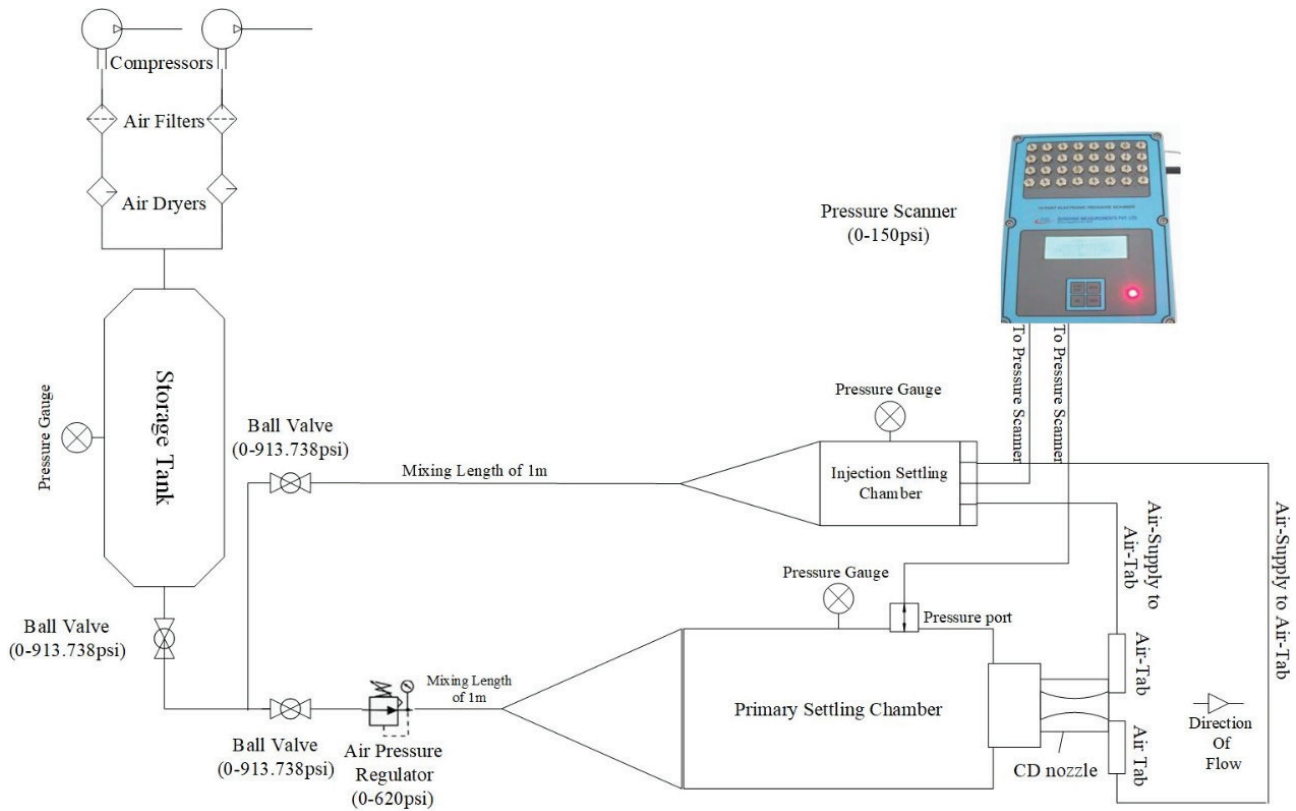


Figure 1. Schematic view of the experimental setup.

study, a circular convergent-divergent nozzle was calibrated to ensure it delivers a supersonic jet of Mach number 2.1. The diameter of the nozzle throat (D_{th}) was 9.6 mm and the nozzle exit diameter (D) was 13.00 mm. The isentropic nozzle pressure ratio (NPR) required for the optimum expansion of the nozzle is 9.14. The pitot pressure distribution along the diameter of the nozzle exit was measured at different NPRs. The pitot pressure (p_{0t}) represents the total pressure downstream of the detached shock at the probe nose. To calculate the flow Mach number, the measured p_{0t} was used in conjunction with the normal shock relation, as given in equation (1) [22]. In the calculation, p_{0s} is assumed to be equal to the settling chamber pressure. The assumption is reasonable since the flow through the nozzle connected to the settling chamber can be considered isentropic.

$$\frac{p_{0t}}{p_{0s}} = \left(\left(1 + \frac{2\gamma}{\gamma+1} (M_e^2 - 1) \right)^{\frac{1}{\gamma-1}} \times \left(\frac{(\gamma+1)M_e^2}{(\gamma-1)M_e^2+2} \right)^{\frac{\gamma}{\gamma-1}} \right) \quad (1)$$

Two constant area tubes of 1 mm inner diameter and 0.1 mm thickness act as air tabs in the experiments. The experiments were done with air tabs positioned diametrically opposite (along Y-axis) at the nozzle exit as shown in Figure 2. An offset of 2 mm is given to the air tabs from the circumference of the nozzle exit to avoid any disturbance to the main jet.

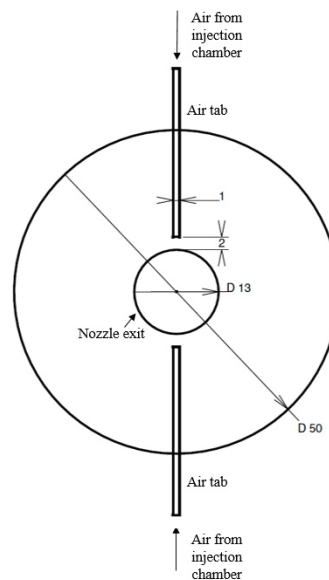


Figure 2. Diagrammatic representation of air tabs position along the jet axis (All dimensions in mm).

Instrumentation

In the jet field, pressure is measured with a pitot probe with an inner diameter of 0.8 mm and thickness of 0.1 mm connected to a pressure scanner. The probe was mounted

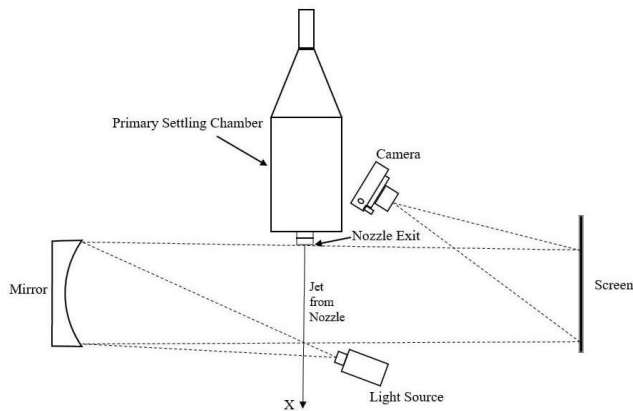


Figure 3. Schematic view of the shadowgraph technique.

on a traverse mechanism (with a linear translation resolution of 0.1 mm) to carry out measurement in all the three directions. The blockage due to probe is said to be negligible if the ratio of the nozzle exit area to the pitot probe area is greater than 64. In the present study, the ratio of nozzle exit area to pitot probe area was 169 (>64). The pressure scanner has a range of 0 - 10.34 bar. The response time of the

pressure scanner is 1ms. The pressure measurement is done at a sampling frequency of 100 Hz which is later averaged to get a single set of pressure. Hence, each measured pressure value in the present study is an average of 100 samples. Shadowgraph technique (Figure 3) is employed to visualize the jet waves. The technique uses a light source, and a parabolic mirror of 200 mm diameter and 2.2 m focal length.

RESULTS AND DISCUSSION

The pressure measurement in this study represents the total pressure behind the detached shock. To obtain the actual total pressure, it is necessary to account for the pressure loss across the shock. However, correcting the measured pitot pressure for the shock-induced losses proves challenging due to variations in Mach number within the core and the varying strength of shock waves in different shock cells. Consequently, obtaining precise values for the actual total pressure becomes difficult. Therefore, it is important to interpret the results obtained for the supersonic jet flow field as qualitative rather than quantitative. While they may not provide precise numerical values, the results are still valuable for comparative purposes. They allow for meaningful comparisons between different cases

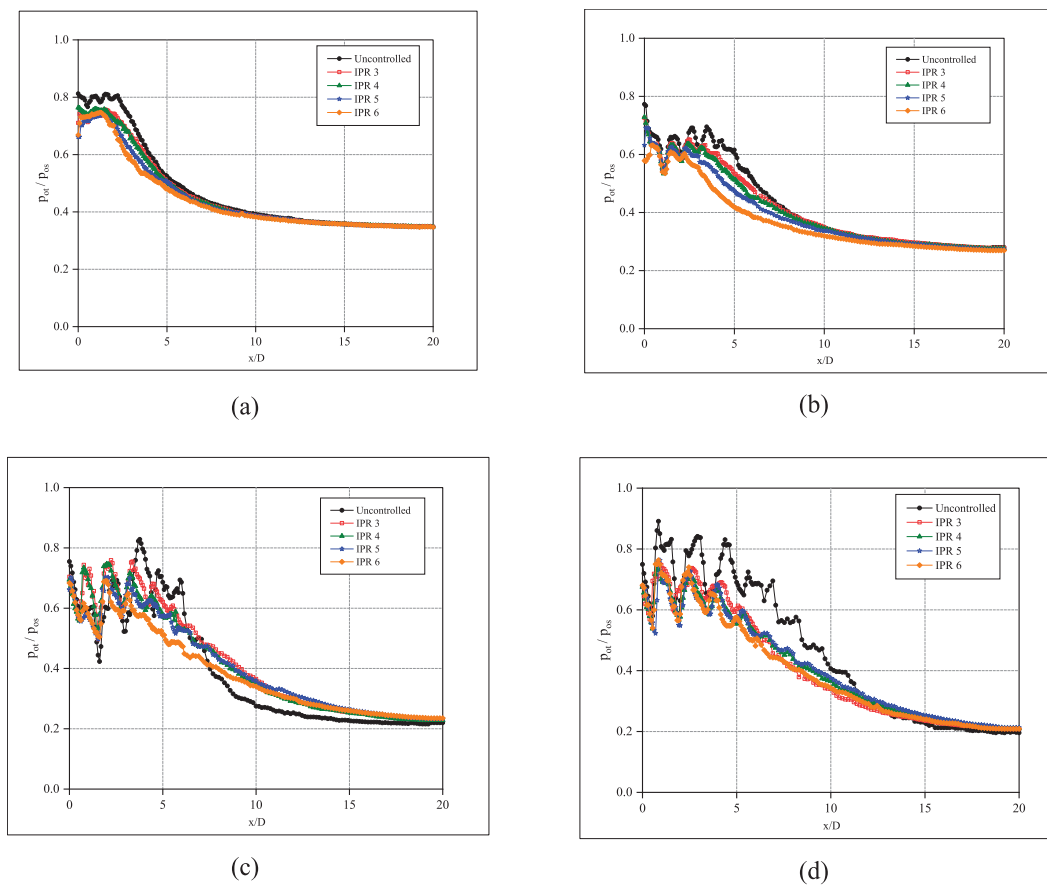


Figure 4. Centerline pitot pressure decay of uncontrolled and controlled jets for air tabs located at $x/D = 0.25$ from nozzle exit for varying IPRs at; (a) NPR 3 (b) NPR 4 (c) NPR 5 (d) NPR 6.

or scenarios under investigation, enabling a qualitative assessment of the impact of the introduced air tabs on the jet flow field.

Centreline Pressure Decay

Centreline pressure decay measurements quantify both the length of the jet core and the decay of characteristic far-field zones in the jet. The pitot pressure variations were measured at intervals of 1 mm along the jet axis, up to 20D of the nozzle diameter. The centreline pressure decay indicates the degree of mixing between the jet and the surrounding medium. By analyzing the pitot pressure decay along the centreline, it is possible to estimate the length of the supersonic core. In supersonic jets, the core does not maintain a constant velocity or Mach number due to the presence of waves. These waves cause oscillations in the pitot pressure within the supersonic core region. Even in jets that are correctly expanded, these waves persist due to the relaxation effect.

To evaluate the impact of air tabs on jet mixing, the measured data of pitot pressure (p_{0t}) along the centreline of the jet are normalized with respect to the stagnation pressure (p_{0s}). The distance along the jet axis (X) is also normalized with respect to the nozzle diameter (D). The pressure decay of both an uncontrolled jet and a jet controlled with an air tab located at 0.25D from the nozzle exit were plotted for various IPRs of 3, 4, 5, and 6 while maintaining fixed NPRs of 3, 4, 5, and 6.

Figure 4 (a) presents the centerline pressure decay plot for NPR 3. In this highly overexpanded condition, the core length values for IPRs of 3, 4, 5, and 6 were determined to be 1.54D, 1.46D, 1.46D, and 1.31D, respectively. Comparatively, the uncontrolled jet exhibited a core length of 2.23D. The percentage reduction in core length for IPRs 3, 4, 5, and 6 amounted to 30.9%, 34.5%, 34.5%, and 41.3%, respectively. Notably, the core length reduction increased with higher IPR values, and the controlled jet showcased shorter pressure oscillations in the near field. The highest core length reduction of 41.3% was observed at IPR 6, emphasizing significant jet mixing characteristics.

Figure 4 (b) illustrates the centerline pressure decay plot for NPR 4. Under highly overexpanded conditions, the core length values for IPRs 3, 4, 5, and 6 were 3.38D, 3.31D, 2.31D, and 2.23D, respectively. The uncontrolled jet had a core length of 5.69D. The percentage reduction in core length for IPRs 3, 4, 5, and 6 reached 40.6%, 41.8%, 59.4%, and 60.8%, respectively. Increasing IPR resulted in a higher core length reduction, and there was a noticeable increase in pressure oscillations in the near field when moving from NPR 3 to 4. The maximum core length reduction of 60.8% was observed at IPR 6.

Figure 4 (c) exhibits the centerline pressure decay plot for NPR 5, where the jet is in an overexpanded condition. The core length values for IPRs 3, 4, 5, and 6 were found to be 5.62D, 5.54D, 5.38D, and 4.00D, respectively. The uncontrolled jet displayed a core length of 7.10D. The

percentage reduction in core length for IPRs 3, 4, 5, and 6 amounted to 20.8%, 22.0%, 24.2%, and 43.7%, respectively. As with previous cases, higher IPR values yielded increased core length reduction, and there was a pronounced increase in pressure oscillations in the near field as NPR increased from 4 to 5. The maximum core length reduction of 43.7% was observed at IPR 6.

Figure 4 (d) showcases the centerline pressure decay plot for NPR 6, where the jet is in an overexpanded condition. The core length values for IPRs 3, 4, 5, and 6 were determined to be 8.92D, 7.69D, 6.62D, and 6.08D, respectively. The uncontrolled jet exhibited a core length of 10.76D. The percentage reduction in core length for IPRs 3, 4, 5, and 6 reached 17.1%, 28.5%, 38.5%, and 43.5%, respectively. As observed previously, increasing IPR values led to greater core length reduction, and there was an evident increase in pressure oscillations in the near field as NPR increased from 5 to 6. The maximum core length reduction of 43.5% was observed at IPR 6.

From Figures 4 (a) to (d), it can be inferred that, for a fixed NPR, an increase in IPR results in a higher percentage reduction in core length. The reduction in core length can be attributed to the increased momentum injection by the air tab, which enhances mixing by generating streamwise vorticity in the main jet and altering the downstream shock cell structure. This mixing promotion weakens shock waves in the near field of the jet.

The introduction of fluidic injection into the main jet creates counter-rotating vortex pairs (CVPs) having opposite rotational directions. The induced velocities of the CVPs initiate their movement towards the centre axis of the main jet. When the CVPs approach closely to each other, their induced velocities grow stronger and distort the main jet leading to the formation of longitudinal vortices spreading in the streamwise direction. Due to the presence of the longitudinal vortices, the ambient fluid is entrained into the jet core leading to enhanced jet mixing. Jet mixing promotes the interaction between the fuel and the surrounding air, leading to more efficient combustion [7].

Arun Kumar et al. [18] have studied the control of sonic circular jets using air tabs. They indicated that the distortion caused by the air tabs increased as the Mach number and mass flow rate increased, while it decreased with a decrease in the diameter of the air tabs. Notably, they achieved a reduction in core length of approximately 76% and 82% when the Mach number of the controlled jet was increased to 1.56 and 1.71, respectively. In another study, Arun Kumar et al. [7], manipulated a Mach 2 jet using convergent and convergent-divergent injectors. They reported a significant effect on the core length of the controlled jet by the mass flow rate ratio of the mini jets to the main jet, the expansion ratio, and the type of injector. The maximum reduction in core length was achieved under the design condition compared to the off-design condition of the manipulated jet. Furthermore, in an empirical scaling analysis of Mach 2 jet control using steady fluidic injection,

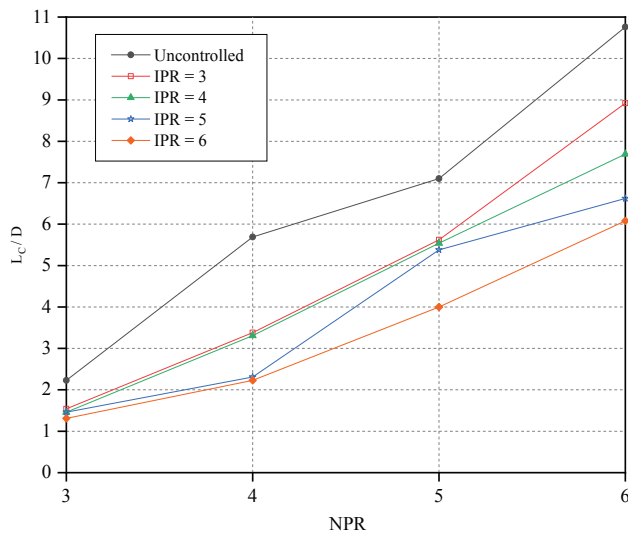


Figure 5. Corelength Variation with NPR for air tabs located at $x/D = 0.25$ from nozzle exit for the uncontrolled and controlled jet.

Arun Kumar et al. [9] have observed a decrease in the core length of the jet with an increase in the mass flow ratio of the mini jet to the main jet for all pressure ratios. Also, a reduction in core length and enhanced mixing was caused by the fluidic injection.

In addition to enhancing mixing, fluidic injectors efficiently disrupt the shock cells in the downstream of the nozzle exit. Shock cells are structures that arise due to the interaction between the high-velocity jet and the surrounding air. By disrupting these shock cells, the injectors influence the shape and intensity of the shock cells. The disruption of the shock cells has a positive effect on noise reduction. It reduces the interaction between the shear layer (the region of flow with a velocity gradient) and the shock cells. This reduction in interaction leads to a decrease in broadband shock-associated noise (BBSAN) compared to the case without fluidic injection. Consequently, there is an overall reduction in the sound pressure level (OASPL), which corresponds to a decrease in the perceived noise level [7].

Corelength Variation with Injection Pressure Ratio

Figure 5 illustrates the variation in core length as a function of nozzle pressure ratio (NPR). It can be observed that the core length increases with an increase in NPR for both uncontrolled and controlled jets. The core length of the uncontrolled jet was found to increase as NPR increased. Similar observations were made for the controlled jets with injection pressure ratios (IPRs) of 3, 4, 5, and 6. However, the core length of the uncontrolled jet was consistently the highest among all NPRs when compared to the controlled jets. The shortest core length was observed in the controlled jet with an IPR of 6.

For NPR 3, the core lengths of the uncontrolled jet and controlled jets with IPRs 3, 4, 5, and 6 were 2.23, 1.54, 1.46, 1.46, and 1.31, respectively. At NPR 4, the core lengths for the uncontrolled jet and controlled jets with IPRs 3, 4, 5, and 6 were 5.69, 3.38, 3.31, 2.31, and 2.23 respectively. The core lengths for NPR 5 were 7.1, 5.62, 5.54, 5.38, and 4.00 for the uncontrolled jet and controlled jets with IPRs 3, 4, 5, and 6. Finally, for NPR 6, the core lengths for the uncontrolled jet and controlled jets with IPRs 3, 4, 5, and 6 were 10.76, 8.92, 7.69, 6.62, and 6.08 respectively.

The graph indicates that an increase in IPR leads to a reduction in core length for a fixed NPR. This reduction can be attributed to the increased momentum injection by the air tab as IPR increases, promoting mixing by generating streamwise vorticity in the main jet and altering the structure of downstream shock cells. This enhanced mixing weakens shock waves in the near field of the jet. Additionally, an increase in NPR results in an increased core length due to greater momentum in the primary jet.

In supersonic jets, Wan and Yu [19] investigated the application of air tabs for Mach number of 1.3 jet and reported that the air tabs resulted in faster decay of the jet centerline velocity, thereby increasing the entrainment of mass flux within the jet. Cuppoletti et al. [20] examined a Mach 1.56 jet and showed the effect of fluidic injection into the shear layer of the main jet, leading to a faster reduction of the potential core. In underexpanded supersonic jets, radial secondary injections should be limited to four or less for optimal mixing [12]. Chauvet et al. [12] demonstrated that the longitudinal vortices strongly influence the mixing efficiency in a distorted jet caused by radial injections. In underexpanded jet controlled by radial injections the shock wave structure resembled a Mach disk due to transverse mass flows [21]. In Mach 2.0 jet manipulated using rectangular tabs, three types of flow categories were identified i.e., the “jet bifurcation”, “complex and strong shock-cell structure” and “weak shock structure”, wherein positioning the tab downstream of the first shock cross-over point resulted in shorter core length and higher jet mixing [4].

Radial Profiles of Pitot Pressure Measurements

Pitot pressure is a measure of the dynamic pressure exerted by the jet that is used to assess the airflow characteristics. Measuring the pitot pressure distribution along the z -direction and y -direction can provide insights into the effects of control on jet symmetry and mixing. By measuring the pitot pressure distribution along the z -direction the jet’s axial symmetry can be evaluated. An ideally symmetric jet would exhibit a uniform pitot pressure distribution along the z -axis. However, if there is asymmetry in the control, it may cause variations in the pitot pressure distribution, indicating deviations from axial symmetry. Pitot pressure measurements provide insights into the radial distribution of pitot pressure and illustrate the changes in flow behaviour as the distance from the nozzle exit increases.

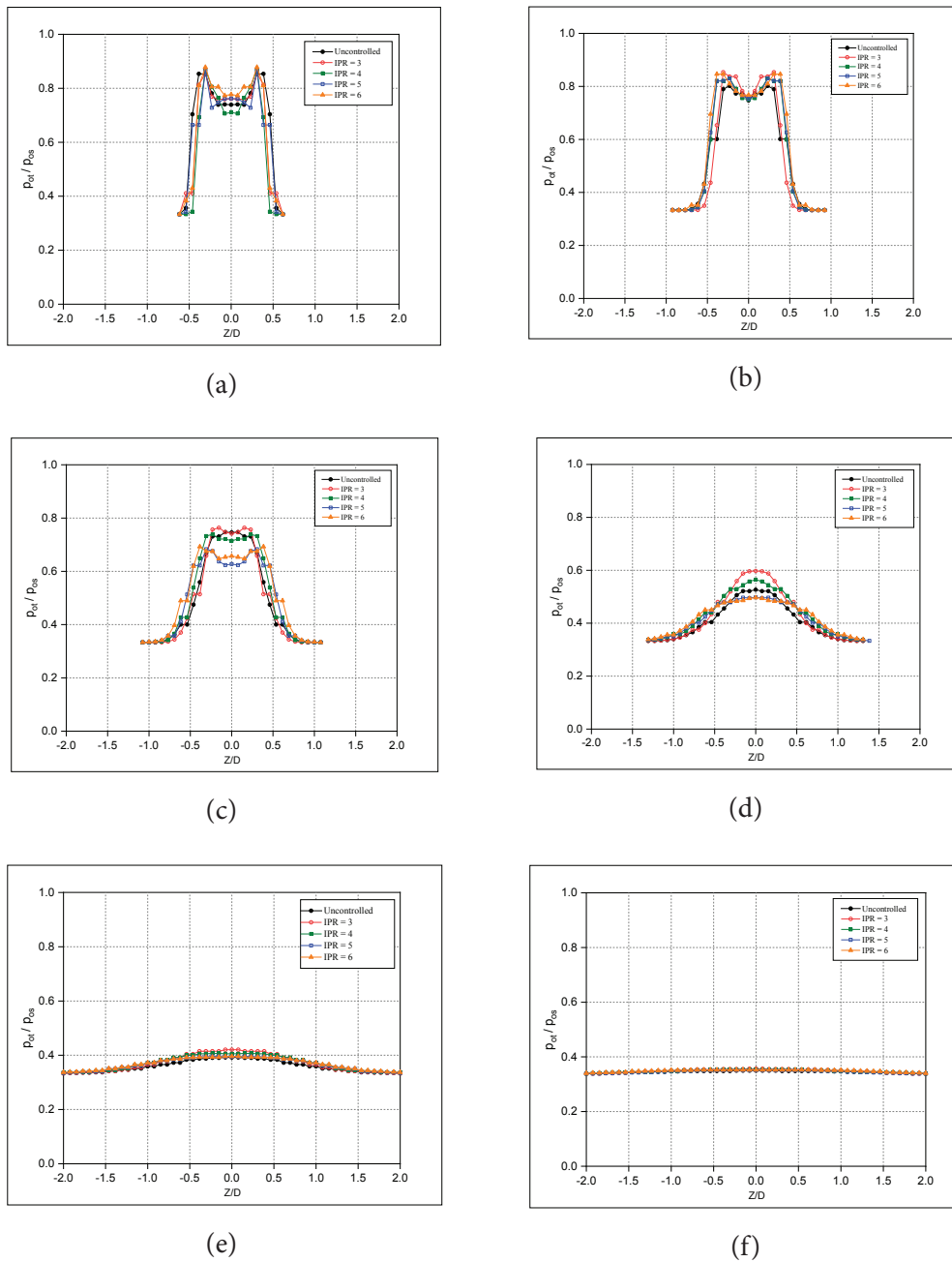


Figure 6. Radial pitot pressure profiles for the uncontrolled and controlled jet at NPR 3, measured at 0.25D. The figures (a) to (f) correspond to different locations along the x-axis normalized by the nozzle diameter (D): (a) $x/D = 0$; (b) $x/D = 1$; (c) $x/D = 2$; (d) $x/D = 4$; (e) $x/D = 8$; (f) $x/D = 16$.

The study involved measuring the pitot pressure distribution along the z-axis at various locations ($x/D = 0, 1, 2, 4, 8, \text{ and } 16$) for different IPR values, namely 3, 4, 5, and 6. These measurements were conducted for corresponding NPRs of 3, 4, 5, and 6 as well.

Figure 6 presents the pitot pressure distribution along the z-axis at different locations ($x/D = 0, 1, 2, 4, 8, \text{ and } 16$) for IPRs 3, 4, 5, and 6, with a corresponding NPR of 3. In Figures 6a, 6b, and 6c, the presence of shock waves in the

near field of the jet is evident. These shock waves signify abrupt changes in pressure and flow characteristics that significantly affect the jet’s behaviour. Progressing downstream along the jet axis, as depicted in Figures 6d, 6e, and 6f, the influence of jet mixing becomes more apparent. The jet undergoes mixing with the surrounding medium, resulting in spreading and dispersion over a larger area. Notably, IPR 6 exhibits accelerated mixing and a reduction in the jet’s core length. This indicates that IPR 6 enhances

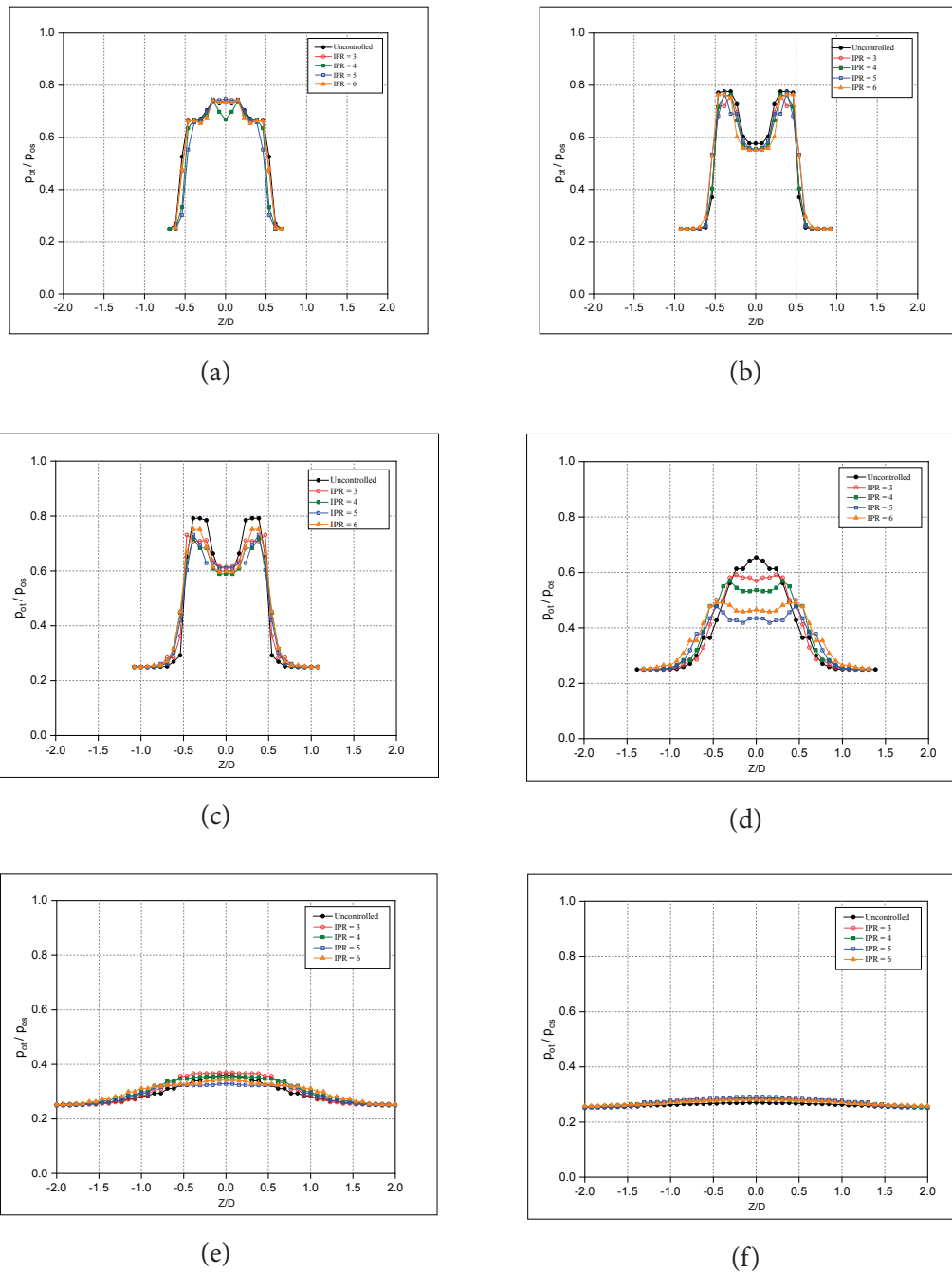


Figure 7. Radial pitot pressure profiles for the uncontrolled and controlled jet at NPR 4, measured at $0.25D$. The figures (a) to (f) correspond to different locations along the x -axis normalized by the nozzle diameter (D): (a) $x/D = 0$; (b) $x/D = 1$; (c) $x/D = 2$; (d) $x/D = 4$; (e) $x/D = 8$; (f) $x/D = 16$.

the efficiency of jet mixing with the surrounding medium, leading to a shorter core length.

In Figure 7, the distribution of pitot pressure along the z -axis at various locations along the x -axis for IPRs 3, 4, 5, and 6, corresponding to a fixed NPR of 4 is illustrated. In Figures 7a, b, c, and d, shock waves persist until $x/D = 4$, consistent with the pressure decay observed along the

centerline. Similar to Figure 6, shock waves are observed in the near field of the jet, while further downstream along the jet axis, jet mixing and spread are noticeable. As the distance along the jet axis increases, the jet spread becomes more pronounced, accompanied by a significant pressure drop. This pressure drop indicates effective jet mixing facilitated by the introduction of an air tab. The degree of jet

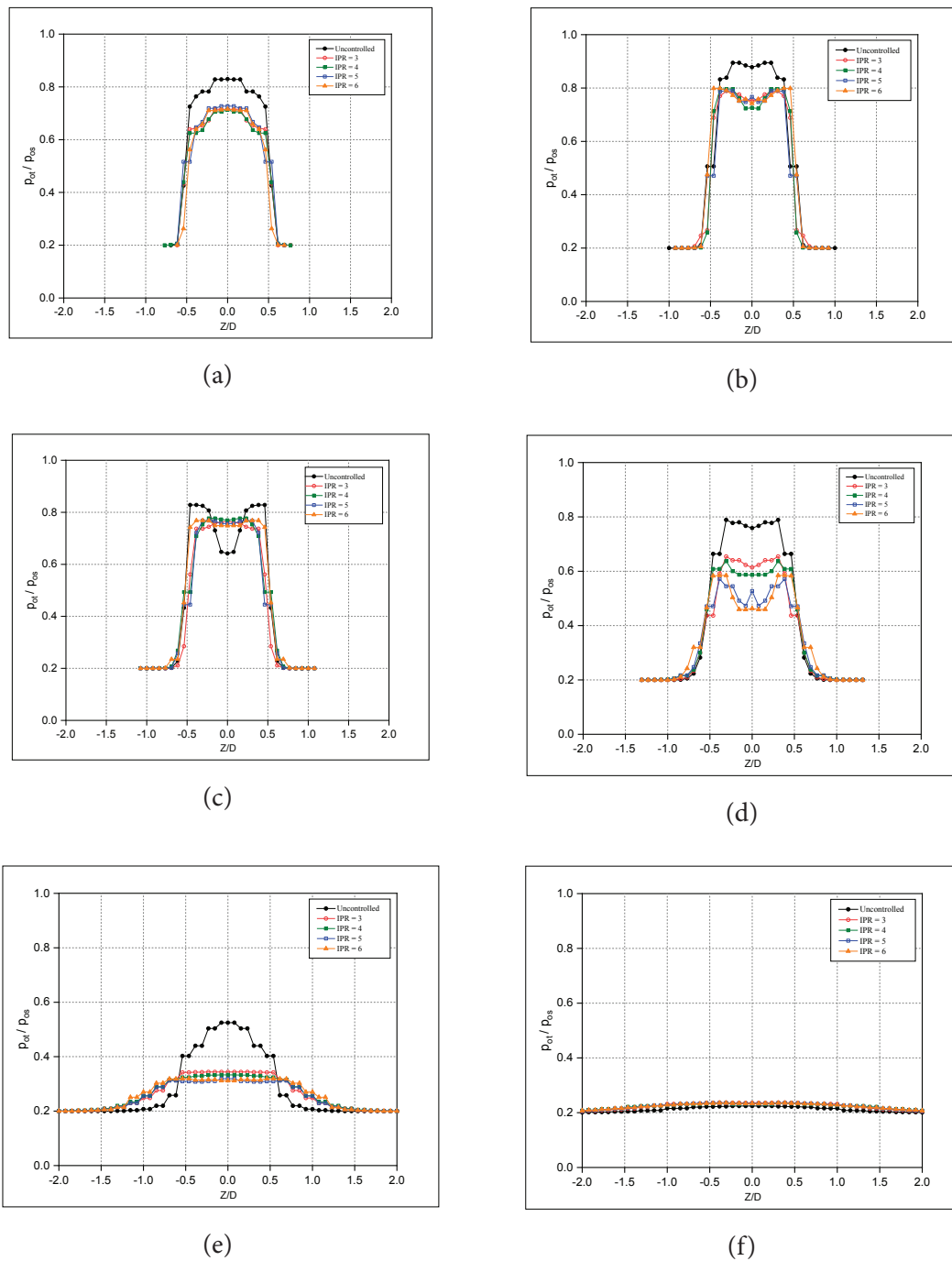


Figure 8. Radial pitot pressure profiles for the uncontrolled and controlled jet at NPR 5, measured at 0.25D. The figures (a) to (f) correspond to different locations along the x-axis normalized by the nozzle diameter (D): (a) $x/D = 0$; (b) $x/D = 1$; (c) $x/D = 2$; (d) $x/D = 4$; (e) $x/D = 8$; (f) $x/D = 16$.

mixing becomes more prominent with higher IPR values. Notably, IPR 6 demonstrates substantial jet mixing and a reduction in the jet’s core length compared to the other IPR values investigated.

The distribution of pitot pressure along the x-axis for IPR values of 3, 4, 5, and 6, with a fixed NPR of 5 is presented in Figure 8. The plots reveal shock waves in the

uncontrolled jet until $x/D = 7$, while in the controlled jets, the shock waves persist until $x/D = 5$. As we proceed downstream along the jet axis, the visualization illustrates jet mixing and spread phenomena. Consistent with previous findings, an increase in the distance along the jet axis leads to a noticeable jet spread accompanied by a significant pressure drop. This drop indicates effective jet mixing, which

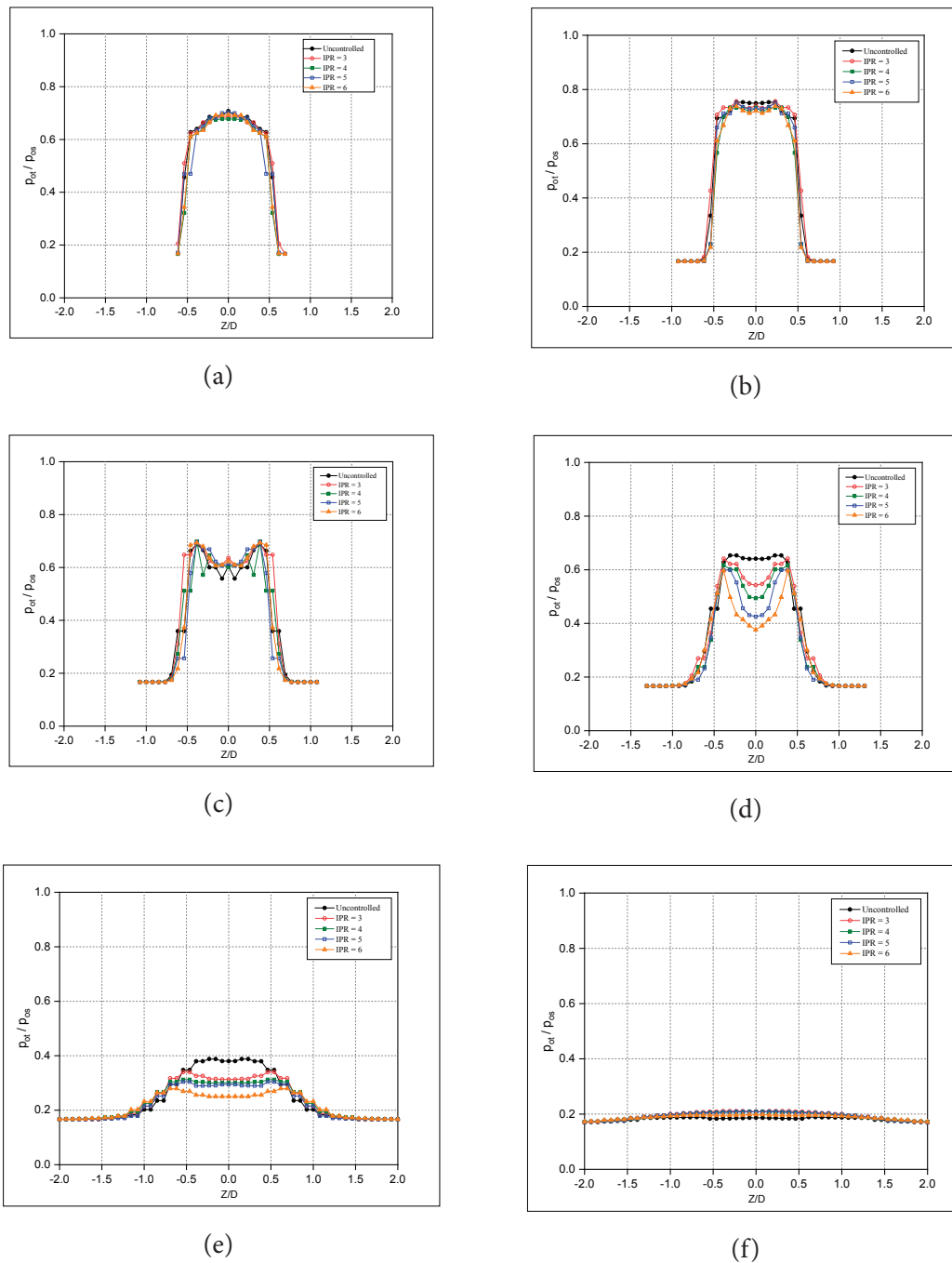


Figure 9. Radial pitot pressure profiles for the uncontrolled and controlled jet at NPR 6, measured at $0.25D$. The figures (a) to (f) correspond to different locations along the x -axis normalized by the nozzle diameter (D): (a) $x/D = 0$; (b) $x/D = 1$; (c) $x/D = 2$; (d) $x/D = 4$; (e) $x/D = 8$; (f) $x/D = 16$.

is facilitated by the introduction of an air tab. Moreover, as the IPR increases, the degree of jet mixing becomes more pronounced. Notably, IPR 6 demonstrates notable jet mixing and a reduction in the core length of the jet compared to uncontrolled jet.

Furthermore, Figure 9 displays the pitot pressure distribution along the z -axis at various locations ($x/D = 0, 1,$

$2, 4, 8,$ and 16) for IPRs 3, 4, 5, and 6, with a corresponding NPR of 6. The plots clearly show that shock waves are more pronounced in the uncontrolled jet compared to the controlled jet. In Figures 9a, b, c, d, and e, shock waves are visible until $x/D = 10$ in the uncontrolled jet, whereas in the controlled jets, the shock waves persist only until $x/D = 5$. As we increase x/D , IPR 6 exhibits a significant pressure

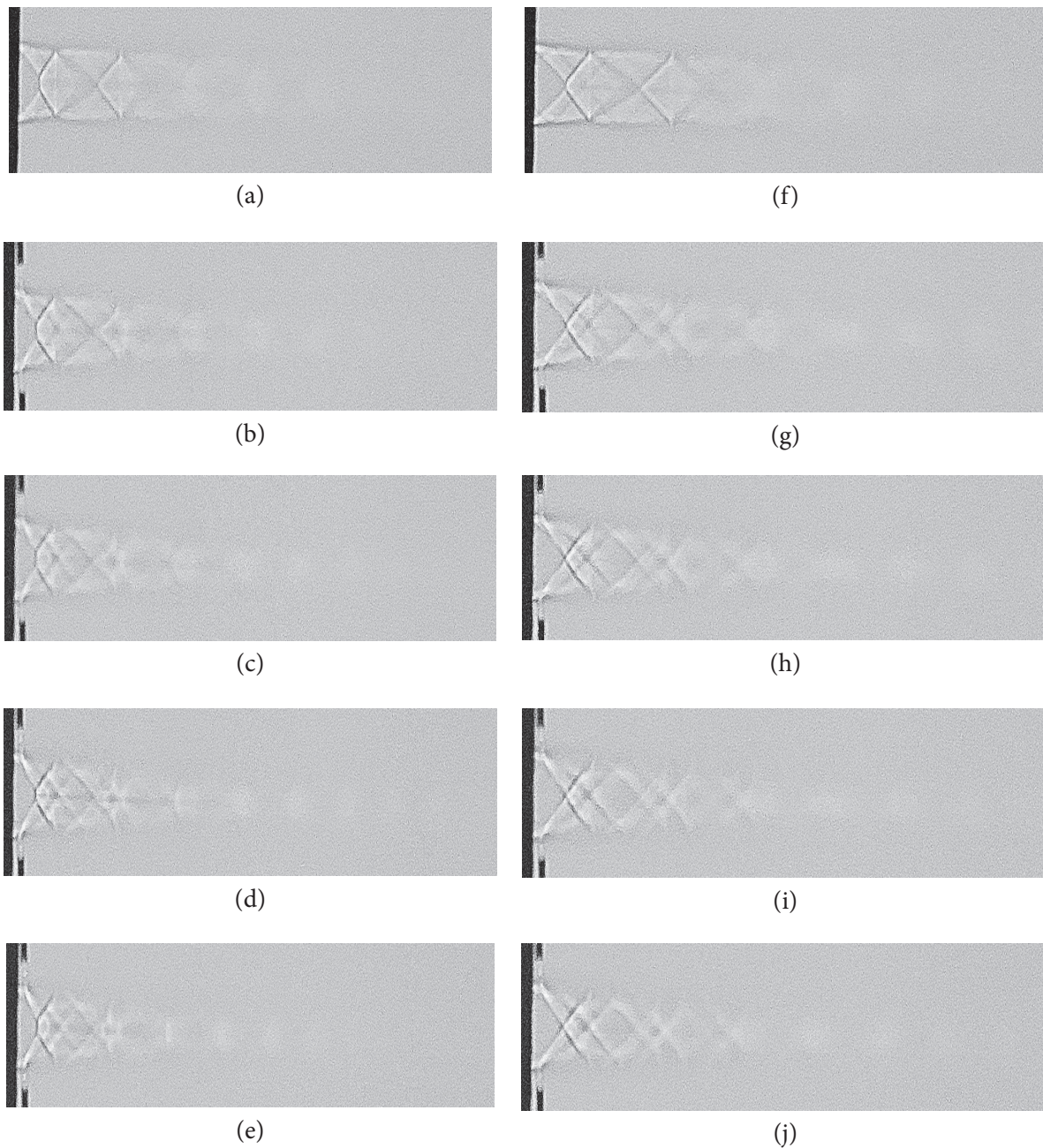


Figure 10. Shadowgraph images of uncontrolled and controlled jet with air tabs located at 0.25 D from nozzle exit (a) Uncontrolled jet at NPR 5 (b) jet with IPR 3 at NPR 5 (c) jet with IPR 4 at NPR 5 (d) jet with IPR 5 at NPR 5 (e) jet with IPR 6 at NPR 5 (f) Uncontrolled jet at NPR 6 (g) jet with IPR 3 at NPR 6 (h) jet with IPR 4 at NPR 6 (i) jet with IPR 5 at NPR 6 (j) jet with IPR 6 at NPR 6.

drop compared to the uncontrolled jet and the other IPRs of the controlled jet. Furthermore, the shock strength decreases with an increase in IPR. Consistent with previous figures, an increase in the distance along the jet axis leads to noticeable jet spread, accompanied by a substantial drop in pressure, indicating effective jet mixing due to the introduction of an air tab.

In summary, the radial pitot pressure plots clearly demonstrate that as the IPR increases, there is a corresponding

significant increase in the pressure drop within the jet. This indicates that higher IPR values lead to more pronounced pressure variations, highlighting the enhanced mixing of the injected flow with the primary flow. Additionally, as the NPR increases from 3 to 6, there is a notable and substantial increase in the pressure drop. This signifies that higher NPR values result in more effective jet mixing. The increased pressure drop suggests that the injected flow interacts more vigorously with the surrounding medium,

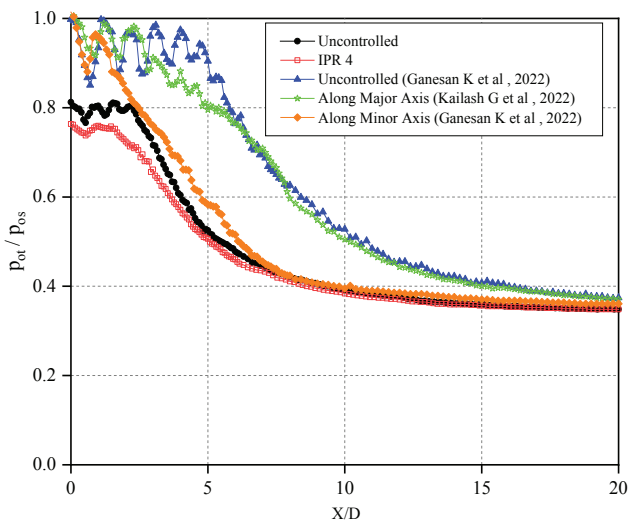


Figure 11. Comparative plots of centreline pitot pressure decay of uncontrolled and controlled jets with Kailash et al. [24].

leading to enhanced jet spreading and dispersion. This phenomenon indicates a higher degree of mixing between the jet and its environment.

Flow Visualization

The shadowgraph images of the supersonic jet (Mach 2.1) were obtained by varying the injection pressure ratio (IPR) from 3 to 6 for a fixed nozzle pressure ratio (NPR) of 3 to 6 and were compared with uncontrolled jet (without fluidic injection). Shadowgraph images for selected NPRs 5 and 6 are shown in Figure 10. NPR 5 and 6 correspond to overexpanded levels of the supersonic jet as its designed NPR is 9.14. The shadowgraph images captured were used to quantify the core lengths of uncontrolled and controlled jets (with fluidic injection). The length of the supersonic core is defined as the axial extent up to which the supersonic flow prevails in the jet field [22]. In this study, the axial extent of waves in the shadowgraph image was taken as the supersonic core length for the circular supersonic jet of Mach No. 2.1. Therefore, it must be noted that the measured core lengths using shadowgraph images are qualitative.

Figure 10a and 10f corresponds to shadowgraph images of the uncontrolled jet at NPR 5 and NPR 6. Figure 10b to 10e and Figure 10g to 10j represent the controlled jet at NPR 5 and NPR 6 for IPRs 3 to 6 respectively. It is observed that the introduction of air tabs alters the shock cell structure in the near field of the jet flow. With an increase in IPRs, the shock waves become weaker promoting faster jet decay resulting in shorter core lengths. The results drawn from these images are in line with the centreline pressure decay plots.

In summary, the fluidic injection or air tab manipulation of the Mach 2.1 jet resulted in a significant improvement of jet mixing and thrust vectoring enhancement with

an increase in IPR as evident from the shadowgraph images of the controlled and uncontrolled jets. Kailash and Aravind Kumar [23] have reported that the core length measurement from the shadowgraph images have indicated that the jet mixing increases with increase in IPR due to the core length reduction in the controlled jet injected along the minor axis [24]. Dhinakaran and Bose [25], reported that an increase in IPR results in a longer upstream separation. Erdem and Kontis [26] also reported that as the IPR was increased, the prominent flow structures extended further in both upstream and downstream directions. [2]. Das et al. [2] have reported that in overexpanded jet, the placement of the fluidic injector or the mini-jet at or near the onset of the overexpansion is of limited or no utility.

In general, the introduction of fluidic injection or air tab into the main jet Mach 2.1 generated counter-rotating vortex pairs (CVPs), which moved towards the main jet axis with its own velocity. When the CVPs are close enough their velocity becomes stronger and distorts the main jet. The distortion of main jet forms longitudinal vortices moving along the streamwise direction and entraining the surrounding ambient fluid into the jet core thereby, enhancing jet mixing.

Comparative Analysis of the Present Study with the Literature

In Figure 11, a comparative plot is depicted, showcasing the outcomes of our study in comparison to the research conducted by Kailash et al. [24]. In their investigation, they studied a rectangular sonic jet with an aspect ratio of 2. They employed sonic fluidic injection through two air tabs positioned diametrically opposite to each other along both the minor and major axes of the nozzle exit. By introducing an air tab along the minor axis with NPR 3 and IPR 4, the potential core length was reduced from 4.8D to 1.1D. Similarly, the introduction of air tabs along the major axis led to a reduction in the potential core length from 4.8D to 4.6D. Interestingly, in our study, when employing an air tab at the nozzle exit with IPR 4 and NPR 3 for controlling a circular jet at Mach 2.1, the potential core length decreased from 2.23D to 1.46D. These results align with the findings of research conducted by Kailash et al. [24]. Such alignment in findings strengthens the broader understanding of the efficacy of air tabs in altering supersonic jet characteristics across different geometries and flow conditions.

CONCLUSION

In conclusion, this investigation has unequivocally established the substantial positive impact of introducing air tabs on enhancing mixing within the primary jet when compared to an uncontrolled jet. The core length of the jet consistently decreases as the injection pressure ratio (IPR) increases for the investigated NPRs of 3, 4, 5, and 6. The percentage reduction in core length becomes more pronounced as the IPRs increase for all NPRs, primarily due to the increased

momentum injection facilitated by the air tab. This augmented momentum injection generates streamwise vorticity within the main jet and modifies the downstream shock cell structure, resulting in enhanced mixing. As a result of this mixing promotion, the strength of shock waves in the vicinity of the jet's exit is mitigated. For NPR 3, the percentage reduction in core length for IPRs 3, 4, 5, and 6 ranges from 30.9% to 41.3%. For NPR 4, the percentage reduction in core length varies from 40.6% to 60.8%. Similarly, for NPR 5, the percentage reduction in core length ranges from 20.8% to 43.7%. For NPR 6, the percentage reduction in core length varies from 17.1% to 43.5%. These results clearly show the significant impact of air tabs in enhancing jet mixing and reducing the core length of the jet, particularly at higher IPRs. The demonstrated potential for enhancing jet performance and reducing noise provides valuable insights for future applications. Moreover, the findings pave the way for further exploration of supersonic air tabs under optimized and expanded jet conditions, promising advancements in the field of aerodynamics and fluid dynamics. This study not only contributes to the scientific knowledge base but also opens avenues for practical applications that can revolutionize supersonic jet technology.

AUTHORSHIP CONTRIBUTIONS

All authors contributed to the study conception and design. Methodology, Material preparation and data collection were performed by [Mahendra Perumal G], [Aravindh Kumar S M]. The first original draft of the manuscript was written by [Mahendra Perumal G]

DATA AVAILABILITY STATEMENT

The authors confirm that the data that supports the findings of this study are available within the article. Raw data that support the finding of this study are available from the corresponding author, upon reasonable request.

CONFLICT OF INTEREST

The authors declare that they have no known competing financial interests or personal relationships that could have appeared to influence the work reported in this paper.

ETHICS

There are no ethical issues with the publication of this manuscript.

REFERENCES

- [1] Khan A, Rao AN, Baghel T, Perumal AK, Kumar R. Parametric study and scaling of Mach 1.5 jet manipulation using steady fluidic injection. *Phys Fluids* 2022;34:036107. [\[CrossRef\]](#)
- [2] Das AK, Acharyya K, Mankodi TK, Saha UK. Fluidic thrust vector control of aerospace vehicles: State-of-the-art review and future prospects. *J Fluids Eng* 2023;145:080801. [\[CrossRef\]](#)
- [3] Kumar PA, Rathakrishnan E. Truncated triangular tabs for supersonic-jet control. *J Propuls Power* 2013;29:50–65. [\[CrossRef\]](#)
- [4] Arun Kumar P, Aileni M, Rathakrishnan E. Impact of tab location relative to the nozzle exit on the shock structure of a supersonic jet. *Phys Fluids* 2019;31:076104. [\[CrossRef\]](#)
- [5] Maruthupandiyam K, Rathakrishnan E. Supersonic jet control with shifted tabs. *Proc Inst Mech Eng Part G J Aeronaut Eng* 2018;232:433–447. [\[CrossRef\]](#)
- [6] Hafsteinsson HE, Eriksson LE, Andersson N, Cuppoletti DR, Gutmark E. Noise control of supersonic jet with steady and flapping fluidic injection. *AIAA J* 2015;53:3251–3272. [\[CrossRef\]](#)
- [7] Kumar PA, Kumar SMA, Mitra AS, Rathakrishnan E. Fluidic injectors for supersonic jet control. *Phys Fluids* 2018;30:126101. [\[CrossRef\]](#)
- [8] Davis M. Variable control of jet decay. *AIAA J* 1982;20:606–609. [\[CrossRef\]](#)
- [9] Kumar PA, Kumar SMA, Mitra AS, Rathakrishnan E. Empirical scaling analysis of supersonic jet control using steady fluidic injection. *Phys Fluids* 2019;31:056107. [\[CrossRef\]](#)
- [10] Henderson B. Fifty years of fluidic injection for jet noise reduction. *Int J Aeroacoustics* 2010;9:91–122. [\[CrossRef\]](#)
- [11] Semlitsch B, Mihăescu M. Fluidic Injection scenarios for shock pattern manipulation in exhausts. *AIAA J* 2018;56:4640–4644. [\[CrossRef\]](#)
- [12] Chauvet N, Deck S, Jacquin L. Numerical study of mixing enhancement in a supersonic round jet. *AIAA J* 2007;45:1675–1687. [\[CrossRef\]](#)
- [13] Perumal AK, Zhou Y. Axisymmetric jet manipulation using multiple unsteady minijets. *Phys Fluids* 2021;33:065124. [\[CrossRef\]](#)
- [14] Yu S, Lim KS, Chao W, Goh XP. Mixing enhancement in subsonic jet flow using the air-tab technique. *AIAA J* 2008;46:2966–2969. [\[CrossRef\]](#)
- [15] Green CJ, Foy McCullough JR. Liquid injection thrust vector control. *AIAA J* 1963;1:573–578. [\[CrossRef\]](#)
- [16] Rizzetta DP. Numerical simulation of slot injection into a turbulent supersonic stream. *AIAA J* 1992;30:2434–2439. [\[CrossRef\]](#)
- [17] Sekar TC, Jaswal K, Arora J, Sundararaj R, Kushari A, Acharya A. Nozzle performance maps for fluidic thrust vectoring. *J Propuls Power* 2021;37:314–325. [\[CrossRef\]](#)
- [18] Kumar PA, Verma SB, Rathakrishnan E. Experimental study of subsonic and sonic jets controlled by air tabs. *J Propuls Power* 2015;31:1473–1481. [\[CrossRef\]](#)

-
- [19] Wan C, Yu S. Investigation of air tab's effect in supersonic jets. *J Propuls Power* 2011;27:1157–1160. [\[CrossRef\]](#)
- [20] Cuppoletti D, Perrino M, Gutmark E. Fluidic injection effects on acoustics of a supersonic jet at various mach numbers. 17th AIAA/CEAS Aeroacoustics Conference (32nd AIAA Aeroacoustics Conference), Portland, Oregon, 05-08 June 2011. [\[CrossRef\]](#)
- [21] Chauvet N, Deck S, Jacquin L. Shock patterns in a slightly underexpanded sonic jet controlled by radial injections. *Phys Fluids* 2007;19:048104. [\[CrossRef\]](#)
- [22] Rathakrishnan E. *Applied gas dynamics*. Hoboken, NJ: Wiley; 2010. p. 680.
- [23] Tam CKW. Supersonic jet noise. *Ann Rev Fluid Mech* 1995;27:17–43. [\[CrossRef\]](#)
- [24] Kailash G, Aravindh Kumar SM, Rathakrishnan E. Air-tab orientation effect on underexpanded sonic rectangular jet mixing. *AIAA J* 2022;60:6054–6061. [\[CrossRef\]](#)
- [25] Dhinakaran R, Bose TK. Numerical simulation of two-dimensional transverse gas injection into supersonic external flows. *AIAA J* 1998;36:486–488. [\[CrossRef\]](#)
- [26] Erdem E, Kontis K. Numerical and experimental investigation of transverse injection flows. *Shock Waves* 2010;20:103–118. [\[CrossRef\]](#)